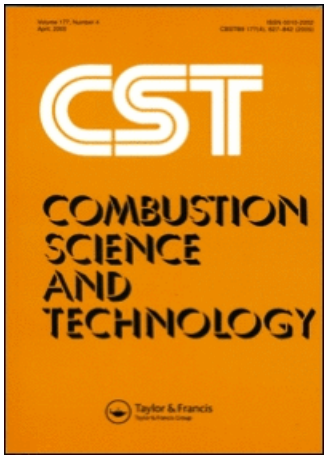

Combustion Science and Technology
Publication details, including instructions for authors and subscription information:
http://www.informaworld.com/smpp/title~content=t713456315

Monte Carlo Calculations of Turbulent Diffusion Flames

T. V. Nguyen [a]; S. B. Pope [a]
[a] Sibley School of Mechanical and Aerospace Engineering, Cornell University, Ithaca, NY

Online Publication Date: 01 January 1984
To cite this Article: Nguyen, T. V. and Pope, S. B. (1984) 'Monte Carlo Calculations of Turbulent Diffusion Flames', Combustion Science and Technology, 42:1, 13 - 45
To link to this article: DOI: 10.1080/00102208408960367
URL: http://dx.doi.org/10.1080/00102208408960367

Combust. Sci. Tech. 1984, Vol. 42, pp. 13-45
0010-2202/84/4202-0013$18.50/0

Monte Carlo Calculations of Turbulent Diffusion Flames

T. V. NGUYEN and S. B. POPE *Sibley School of Mechanical and Aerospace Engineering, Cornell University, Ithaca, NY 14853*

(*Received February 14, 1984; in final form June 7, 1984*)

Abstract—Calculations of turbulent diffusion flames are presented and compared with experimental data. In the calculation procedure, the mean continuity and momentum equations are solved by a finite-difference method, and the k–ε turbulence model is used to model the Reynolds stresses. The conserved-scalar approach is used so that the local, instantaneous, thermochemical properties of the flame are uniquely related to a single conserved scalar $f(x, t)$—the mixture fraction. A modelled transport equation for the probability density function (pdf) of f is solved by a Monte Carlo method.

The results of calculations are compared with experimental data for three turbulent flows: an inert methane jet; a hydrogen/air diffusion flame; and a hydrogen–argon/air diffusion flame. In general there is good agreement between calculated and measured quantities, including pdf's. Numerical tests of the Monte Carlo method are also reported. These demonstrate the convergence of the method and provide an estimate of the statistical error.

1 INTRODUCTION

Turbulent jet diffusion flames have been the subject of several experimental studies: Hawthorne, Weddell and Hottel (1949), Kent and Bilger (1973), and Driscoll, Schefer and Dibble (1982), for example. Such flames are of direct practical importance and at the same time are well suited to the study of fundamental turbulent combustion processes.

Lockwood and Naguib (1975) and Kent and Bilger (1976) have made turbulence-model calculations of diffusion flames. In these calculations, the Reynolds stresses are determined from the turbulent-viscosity hypothesis, with the turbulent viscosity μ_T being obtained from the equation

$$\mu_T = C_\mu \langle \rho \rangle k^2/\varepsilon. \tag{1}$$

Here k is the turbulent kinetic energy, ε is its rate of dissipation, $\langle \rho \rangle$ is the mean density, and the coefficient C_μ is taken to be a constant. Standard modelled transport equations (see Launder and Spalding, 1976) are solved for k and ε. Thus, if the mean density $\langle \rho \rangle$ is known, the continuity, momentum and k–ε equations form a closed set.

Both Lockwood and Naguib (1975) and Kent and Bilger (1976) treated the thermochemistry of the flame by the conserved scalar approach with the assumption that reaction is very rapid compared to the smallest flow or turbulence time scale. In this approach it is assumed that all molecular diffusion coefficients are equal, that the Lewis number is unity, that there is negligible heat loss by radiation, and that the Mach number is low. For then the enthalpy and the mass fraction of each element (in whatever molecular form) are linearly related to a conserved scalar $f(x, t)$. This can be taken to be the jet nozzle fluid concentration (or mixture fraction), and hence $f=1$ in the nozzle, and $f=0$ in the surrounding airstream.

The rapid-reaction assumption implies that, locally, there is chemical equilibrium. The equilibrium state is a function of the pressure, enthalpy and elemental composition. In view of the assumed low Mach number, turbulent pressure fluctuations are very small compared to the mean pressure and hence have a negligible effect on the thermochemical state. Thus for a given mean pressure, the local thermochemical state is uniquely determined by $f(x, t)$, since f uniquely determines the enthalpy and element mass fractions. For any thermochemical quantity—the density, for example—we can then write

$$\rho(x, t) = \rho^*[f(x, t)], \tag{2}$$

where ρ^* is the equilibrium density as a function of f at the given mean pressure.

In order to determine the mean density $\langle \rho(x, t) \rangle$ a knowledge of the mean $\langle f(x, t) \rangle$ is insufficient. But $\langle \rho(x, t) \rangle$—or the mean of any other function of f—can be determined from the probability density function (pdf) of f, $p(\hat{f}; x, t)$. [This is defined as the probability density of the event $f(x, t) = \hat{f}$.] In terms of the pdf, the mean density is

$$\langle \rho(x, t) \rangle = \int_0^1 p(\hat{f}; x, t)\, \rho^*(\hat{f})\, d\hat{f}. \tag{3}$$

(Henceforth the asterisk is omitted: the arguments suffice to indicate whether ρ is being considered a function of $\hat{f}$ or of x and t.)

Lockwood and Naguib (1975) assumed $p(\hat{f}; x, t)$ to be a clipped Gaussian: that is, a Gaussian for $0 \leqslant \hat{f} \leqslant 1$, with the tails of the Gaussian ($\hat{f} < 0$ and $\hat{f} > 1$) lumped into delta functions at $\hat{f} = 0$ and $\hat{f} = 1$. Such an assumed distribution can be uniquely determined from its mean $\langle f \rangle$ and variance $\langle f'^2 \rangle$ for which Lockwood and Naguib solved modelled transport equations. Other authors (*e.g.* Kent and Bilger, 1976; Kolbe and Kollmann, 1980; Rhodes, Harsha and Peters, 1974) have made other assumptions about the shape of the pdf.

Janicka, Kolbe and Kollmann (1978) used a finite-difference method to solve a modelled transport equation for the pdf $p(\hat{f}; x, t)$. This removes the need to assume a pdf shape and is potentially more accurate. In the present work we also use a modelled transport equation for the pdf but solve it by a Monte Carlo method (Pope, 1981a). In contrast to the assumed-pdf method, the pdf-equation approach is readily extended to several reactive (*i.e.* non-conserved) scalars (Pope, 1981b). The Monte Carlo method is essential to such extensions since finite-difference methods are computationally impracticable for joint pdf's of large dimensionality. Consequently an important component of the present work is a numerical study of the Monte Carlo method.

In the next section the model equations are presented. The numerical method is outlined in Section 3 and numerical tests are reported. These tests confirm the convergence of the Monte Carlo method and determine its accuracy and computational cost. In Section 4 results of calculations (including pdf's) are compared with experimental data from three flows: a non-reacting methane jet is quiescent air (Birch, Brown, Dodson and Thomas, 1978); a hydrogen/air diffusion flame (Kent and Bilger, 1973); and, a hydrogen–argon/air diffusion flame (Driscoll, Schefer and Dibble, 1982).

2 MODEL EQUATIONS

We first present the modelled equations for the mean flow and turbulence fields. These equations are for the density-weighted mean velocities

$$\tilde{U}_i \equiv \langle \rho U_i \rangle / \langle \rho \rangle, \tag{4}$$

for the density-weighted turbulent kinetic energy

$$k \equiv \frac{1}{2} \widetilde{u_i'' u_i''}, \tag{5}$$

and for its rate of dissipation ε. Angled brackets denote means, tildes denote density-weighted means, and primes and double primes, respectively, denote the fluctuations about these means. (The equations are presented in their general form, although it is the steady-state boundary-layer equations that are solved.)

The mean equations for the conservation of mass and momentum are

$$\frac{\partial \langle \rho \rangle}{\partial t} + \frac{\partial (\langle \rho \rangle \tilde{U}_i)}{\partial x_i} = 0, \tag{6}$$

and

$$\frac{\partial}{\partial t}(\langle \rho \rangle \tilde{U}_j) + \frac{\partial}{\partial x_i}(\langle \rho \rangle \tilde{U}_i \tilde{U}_j + \langle \rho \rangle \widetilde{u_i'' u_j''}) = -\frac{\partial \langle P \rangle}{\partial x_j}, \tag{7}$$

where P is the pressure. The effects of body forces and viscous stresses have been neglected which is acceptable for the flows considered. The Reynolds stresses are modelled by

$$-\langle \rho \rangle \widetilde{u_i'' u_j''} = \mu_T \left(\frac{\partial \tilde{U}_i}{\partial x_j} + \frac{\partial \tilde{U}_j}{\partial x_i} \right) - \frac{2}{3} \left(\mu_T \frac{\partial \tilde{U}_l}{\partial x_l} + \langle \rho \rangle k \right) \delta_{ij}, \tag{8}$$

where the turbulent viscosity is given by Eq. (1).

The modelled transport equations for k and ε are

$$\frac{\partial}{\partial t}(\langle \rho \rangle k) + \frac{\partial}{\partial x_i}(\langle \rho \rangle \tilde{U}_i k) = \frac{\partial}{\partial x_i}\left(\frac{\mu_T}{\sigma_k} \frac{\partial k}{\partial x_i} \right) + G - \langle \rho \rangle \varepsilon, \tag{9}$$

and

$$\frac{\partial}{\partial t}(\langle \rho \rangle \varepsilon) + \frac{\partial}{\partial x_i}(\langle \rho \rangle \tilde{U}_i \varepsilon) = \frac{\partial}{\partial x_i}\left(\frac{\mu_T}{\sigma_\varepsilon} \frac{\partial \varepsilon}{\partial x_i} \right) + \frac{\varepsilon}{k}(C_{\varepsilon 1} G - C_{\varepsilon 2} \langle \rho \rangle \varepsilon), \tag{10}$$

where G is defined by

$$G = -\langle \rho \rangle \widetilde{u_i'' u_j''} \frac{\partial \tilde{U}_i}{\partial x_j} - \frac{\mu_T}{\langle \rho \rangle^2} \frac{\partial \langle \rho \rangle}{\partial x_i} \frac{\partial \langle P \rangle}{\partial x_i}, \tag{11}$$

and σ_k, σ_ε, $C_{\varepsilon 1}$, $C_{\varepsilon 2}$ and C_μ are model constants whose values are given below. The use of these equations in turbulent reactive flows is discussed by Jones and Whitelaw (1982). They suggest the addition of the last term in Eq. (11) to account for the interaction of mean density and pressure gradients. It is found that, for the three flows considered, the additional term has an insignificant effect on the results.

The density-weighted pdf of f is

$$\tilde{p}(\hat{f}; x, t) \equiv \rho(\hat{f}) p(\hat{f}; x, t)/\langle\rho\rangle. \tag{12}$$

For any function of f, $Q(f)$, the density-weighted mean is then given by

$$\widetilde{Q(f)} = \int_0^1 Q(\hat{f}) \tilde{p}(\hat{f}; x, t)\, d\hat{f}, \tag{13}$$

while the mean density can be obtained from

$$\langle\rho\rangle^{-1} = \int_0^1 [\rho(\hat{f})]^{-1} \tilde{p}(\hat{f}; x, t)\, d\hat{f}. \tag{14}$$

For each flame considered, all thermochemical properties are determined as functions of $\hat{f}$ from the equilibrium code of Gordon and McBride (1971).

The modelled transport equation for $\tilde{p}(\hat{f}; x, t)$ is the same as that used previously by Pope (1981a, b) and by Givi, Sirignano and Pope (1984):

$$\frac{\partial}{\partial t}(\langle\rho\rangle\tilde{p}) + \frac{\partial}{\partial x_i}(\langle\rho\rangle\tilde{U}_i\tilde{p}) = \frac{\partial}{\partial x_i}\left(\frac{\mu_T}{\sigma_f}\frac{\partial\tilde{p}}{\partial x_i}\right) + \langle\rho\rangle E(\hat{f}; x, t). \tag{15}$$

The rate-of-change and mean-convection terms on the left-hand side are exact. Convection by the fluctuating velocity field is modelled as gradient diffusion with coefficient μ_T/σ_f where σ_f is ascribed the value 0.7. In general, the use of gradient-diffusion models in variable-density reactive flows is highly dubious. It can be avoided by considering the joint pdf of velocity and the scalar (Pope, 1981c) for then the turbulent transport term appears in closed form. But for a conserved scalar in a simple shear flow, direct measurements (Driscoll *et al.*, 1982) suggest that the gradient-diffusion model may be acceptable.

The final term in Eq. (15) represents mixing by molecular diffusion. It is modelled by Curl's (1963) coalescence-dispersal model:

$$E(\hat{f}; x, t) = 2\omega \int_0^1 \tilde{p}(\hat{f}+f^*)\tilde{p}(\hat{f}-f^*)\, df^* - \omega\tilde{p}(\hat{f}), \tag{16}$$

where the mixing frequency is

$$\omega = 2C_\phi \varepsilon/k. \tag{17}$$

and the constant C_ϕ is ascribed the value 2.0. The modelling of the mixing term has received considerable attention (Dopazo, 1979; Janicka *et al.*, 1979; Pope, 1982) mainly because all the simple models suggested to date have serious deficiencies. In the present context, the principal deficiency of Curl's model is that it overestimates the flatness factor (and higher normalized moments of the pdf). Pope (1982) has shown that, for the case of decaying scalar fluctuations in homogeneous turbulence, Curl's model causes the flatness factor to increase without limit rather than to tend to the Gaussian value of 3.

In order to compare the present approach to moment methods, it is useful to note that modelled equations for $\tilde{f}$ and $g \equiv \widetilde{f''^2}$ can be obtained from Eqs. (15)–(17):

$$\frac{\partial}{\partial t}(\langle\rho\rangle\tilde{f}) + \frac{\partial}{\partial x_i}(\langle\rho\rangle\tilde{U}_i\tilde{f}) = \frac{\partial}{\partial x_i}\left(\frac{\mu_T}{\sigma_f}\frac{\partial\tilde{f}}{\partial x_i}\right), \tag{18}$$

and

$$\frac{\partial}{\partial t}(\langle\rho\rangle g) + \frac{\partial}{\partial x_i}(\langle\rho\rangle\tilde{U}_i g) = \frac{\partial}{\partial x_i}\left(\frac{\mu_T}{\sigma_f}\frac{\partial g}{\partial x_i}\right) + 2\frac{\mu_T}{\sigma_f}\frac{\partial\tilde{f}}{\partial x_i}\frac{\partial\tilde{f}}{\partial x_i} - C_\phi\langle\rho\rangle\frac{\varepsilon}{k}g. \tag{19}$$

These equations are identical to those used by previous investigators (*e.g.* Lockwood and Naguib, 1975; Kent and Bilger, 1976), and consequently the pdf model constants σ_f and C_ϕ can be related to model constants in the $\tilde{f}$ and g equations.

Our principal aim here is to investigate the performance of the pdf equation and of the Monte Carlo method—not to propose a universal model. Consequently we follow Lockwood and Naguib in selecting one set of model constants for inert flows and another set for reacting flows: these are shown in Table I. (That different constants are needed to produce agreement with experimental data indicates a lack of universality in the model.) A detailed study of the influence of the model constants is given by Nguyen (1984).

In summary, modelled transport equations are solved for $\tilde{U}$, k, ε and $\tilde{p}$, and the mean density is determined from Eq. (14).

TABLE I

Turbulence model constants

	C_μ	C_{ε_1}	C_{ε_2}	C_ϕ	σ_k	σ_ε	σ_f
Inert flows	0.09	1.45	1.9	2.0	1.0	1.3	0.7
Reacting flows	0.09	1.44	1.789	1.789	1.0	1.3	0.7

3 SOLUTION PROCEDURE

In the first two subsections we briefly describe the finite-difference method used to solve the equations for $\tilde{U}$, k and ε, and the Monte Carlo method used to solve the equation for $\tilde{p}$. Extensive numerical tests were performed: some results on the accuracy of the Monte Carlo method are presented in Section 3.3.

3.1 *Finite-Difference Method*

The finite-difference method used has been fully described by Pope (1977a, 1977b). We describe here just the coordinate system and grid arrangement in order to provide the required background to the next two subsections.

Consider the polar-cylindrical coordinates x, r, θ in which x is the dominant flow direction and r is the radial direction. All statistical quantities are independent of the circumferential coordinate θ. In the flows considered, the jet half-width $r_{1/2}(x)$ is defined as the radial position at which the axial velocity $\tilde{U}(x, r)$ is equal to the average of the centerline and free stream velocities: that is,

$$\tilde{U}(x, r_{1/2}) = \frac{1}{2}[\tilde{U}(x, 0) + \tilde{U}(x, \infty)]. \tag{20}$$

The half-width is used to define the normalized axial and radial coordinates

$$X \equiv \int_0^x r_{1/2}^{-1}(x')\, dx', \tag{21}$$

and

$$\eta \equiv r/r_{1/2}(x). \tag{22}$$

Starting from initial conditions at $X = X_0 = 0$, the solution at successive axial locations $X_t = X_{t-1} + \Delta X$ is obtained by a marching procedure. Boundary conditions are imposed on the centerline ($\eta = 0$) and in the freestream or ambient ($\eta = \eta_{\max}$). In the cross-stream direction, finite-difference nodes are located a distance $\Delta\eta$ apart. A complete description of the method is provided by Pope (1977a, b).

The finite-difference scheme contains three numerical parameters: ΔX, $\Delta\eta$ and $\eta_{\max}$. Nguyen (1984) investigated the influence of these parameters and confirmed the convergence of the scheme as ΔX, $\Delta\eta$ and $\eta_{\max}^{-1}$ tend to zero.

3.2 *Monte Carlo Method*

The Monte Carlo method uses the same grid as the finite-difference method. At each node, the pdf $\tilde{p}(\hat{f}; X, \eta)$ is represented indirectly by an ensemble of N representative values of f, $f^{(n)}$ ($n = 1, 2, \ldots, N$). For any function of f, $Q(f)$, the ensemble average is defined by

$$\langle Q(f)\rangle_N \equiv \frac{1}{N}\sum_{n=1}^{N} Q[f^{(n)}]. \tag{23}$$

This ensemble average corresponds to the density-weighted mean of $Q(f)$ in that, as N tends to infinity, $\langle Q(f)\rangle_N$ converges in probability to $\widetilde{Q(f)}$.

Initial conditions are specified at $X = X_0$: if the node is in the jet then $f^{(n)} = 1$ (all n), or if it is in the freestream or ambient then $f^{(n)} = 0$. At the axial location X_t, the representative values $f^{(n)}$ at a given node (at $\eta = \eta_j$, say) are obtained as a linear

combination of the values at the three nearest upstream nodes: these are located at $(X_{i-1}, \eta_j - \Delta\eta)$, (X_{i-1}, η_j) and $(X_{i-1}, \eta_j + \Delta\eta)$. Of course, the precise way in which this is performed defines the Monte Carlo method and the pdf equation that it simulates. Pope (1981a) for the general case, and Nguyen (1984) for the particular case in hand, have described the details of the Monte Carlo method and proved convergence.

The Monte Carlo method introduces the additional numerical parameter N. The above-mentioned convergence proof shows that the ensemble average $\langle Q(f)\rangle_N$ converges in probability to $Q(f)$ as N tends to infinity. But for finite N, $\langle Q(f)\rangle_N$ is a random variable whose standard deviation can be expected to be proportional to $N^{-1/2}$. Thus in the Monte Carlo method, the ensemble average at each node contains some statistical error. This error can be reduced by smoothing the profile across the flow. For the calculations reported in Section 4, mean profiles are determined as least-squares cubic splines (de Boor, 1978) with 20 basis functions. For the calculations reported in Section 3.3, a more sophisticated smoothing cubic spline (Reinsch, 1967) is used with a cross-validation procedure to determine the smoothing parameter. Again, 20 basis functions are used.

3.3 *Numerical Tests*

Numerical tests of the finite-difference scheme have been reported by Pope (1977a) and by Nguyen (1984). Here we report tests to determine the effect of the numerical parameter N in the Monte Carlo method. Calculations were made for Kent and Bilger's hydrogen-air diffusion flame with $\Delta X = 0.1$, $\Delta\eta = 0.154$ and $\eta_{\max} = 4.0$, and with various values of N. About 600 axial steps were needed to reach the selected output station of 80 diameters (*i.e.* $x/d = 80$). At this location the jet half-width $r_{1/2}$ is approximately $3.2d$.

At a given location (X, η) the ensemble average $\langle f\rangle_N$ is a random variable. If the Monte Carlo calculation is performed M times (using different random numbers), then the resulting ensemble averages $\langle f\rangle_{N,m}$ $(m = 1, 2, \ldots, M)$ are different. The expectation of $\langle f\rangle_N$ can be estimated by

$$\langle\langle f\rangle_N\rangle \approx \tilde{f}_N \equiv \frac{1}{M}\sum_{m=1}^{M}\langle f\rangle_{N,m}. \tag{24}$$

Similarly the ensemble average variance $\langle f'^2\rangle_N$ (which approximates $\widetilde{f''^2}$) is also a random variable and its expectation can be approximated by

$$\langle\langle f'^2\rangle_N\rangle \approx (f_N')^2 \equiv \frac{1}{M}\sum_{m=1}^{M}\langle f'^2\rangle_{N,m}. \tag{25}$$

In order to determine the dependence of $\tilde{f}_N$ and f_N' on N, calculations were made for the different values of N, 40, 100, 400, 1,000, 4,000 and 10,000. The corresponding number of runs was $M = 125$, 50, 13, 5, 2 and 2. The number of runs was chosen so that the product $N \times M$ is approximately the same in each case, and consequently the accuracy of the approximations in Eqs. (24) and (25) are about the same.

Radial profiles of $\bar{f}_N$ and f_N' at $x/d=80$ are shown on Figure 1. It may be seen that the centerline value of $\bar{f}_N$ is about 6 percent of its initial value. It appears that for $N \geqslant 100$, the expectations of $\langle f \rangle_N$ and $\langle f'^2 \rangle_N$ depend little upon N, whereas for the smallest number of elements ($N=40$) a difference can be discerned.

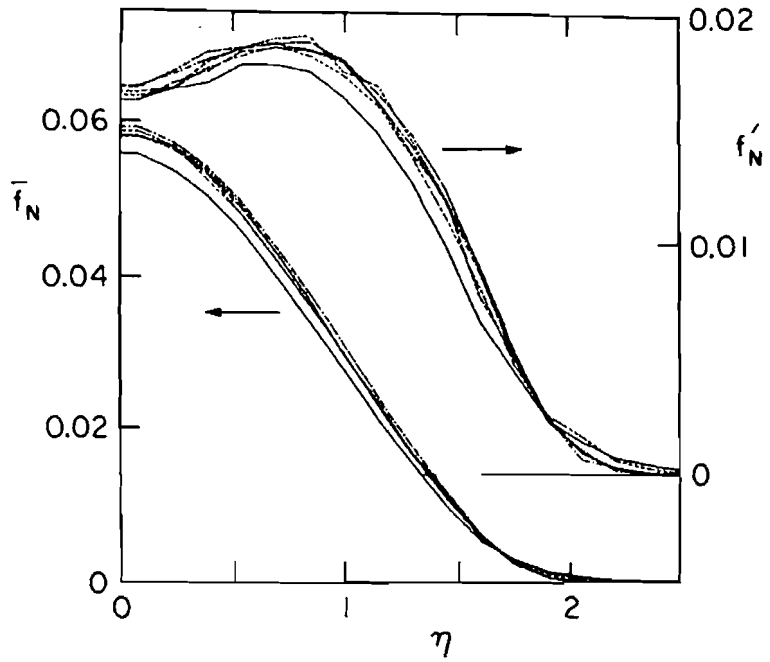

FIGURE 1 Expectations of ensemble-average mean and standard deviation of f against normalized radial distance. $N=40$ ——; $N=100$ - - - - -; N=400 — — —; N=1,000 —·—·—; $N=4{,}000$ ——— ———; $N=10{,}000$ ——— ——— ———.

The standard deviation of $\langle f \rangle_N$ is called the standard error and is approximated by

$$\varepsilon_{st}^2 \equiv \frac{1}{M-1} \sum_{m=1}^{M} (\langle f \rangle_{N,m} - \bar{f}_N)^2. \tag{26}$$

Figures 2 and 3 show ε_{st} plotted against η at $x/d=80$ for different values of N. As expected, the standard error decreases with increasing N. (The statistical error in estimating the standard error is proportional to $M^{-1/2}$. For this reason there is far more scatter in Figure 3 than in Figure 2.)

In order to examine more precisely the effect of the number of elements, Figure 4 shows $\bar{f}_N \pm \varepsilon_{st}$ plotted against $N^{-1/2}$, for three radial locations at $x/d=80$. It appears that the method is slightly biased: that is, $\bar{f}_N$ depends (weakly) on N. This is in contrast to the finding of Pope (1981a) who used the same method but on different flows. The reason for the difference is, most likely, that in the present case the mean

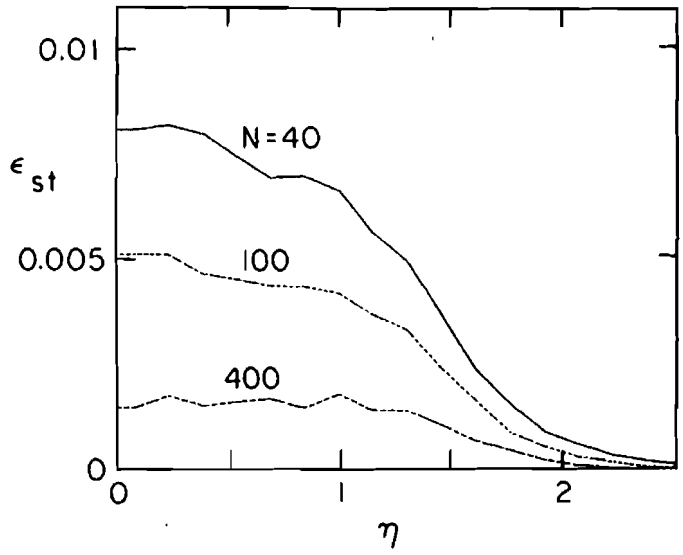

FIGURE 2 Standard error against normalized radial distance.

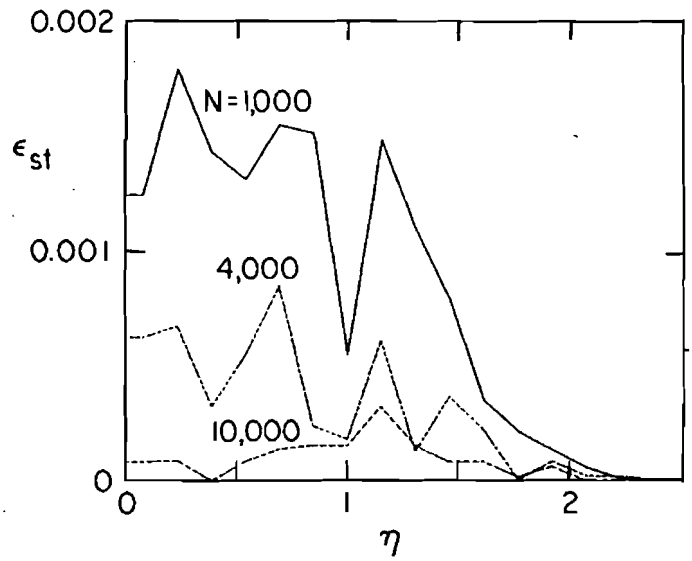

FIGURE 3 Standard error against normalized radial distance.

density is determined from ensemble averages and is therefore subject to statistical error. These statistical errors affect the calculation of the flow field and hence permeate through the whole calculation procedure. However, the small bias is of little consequence since it appears to be negligible for $N \geqslant 100$.

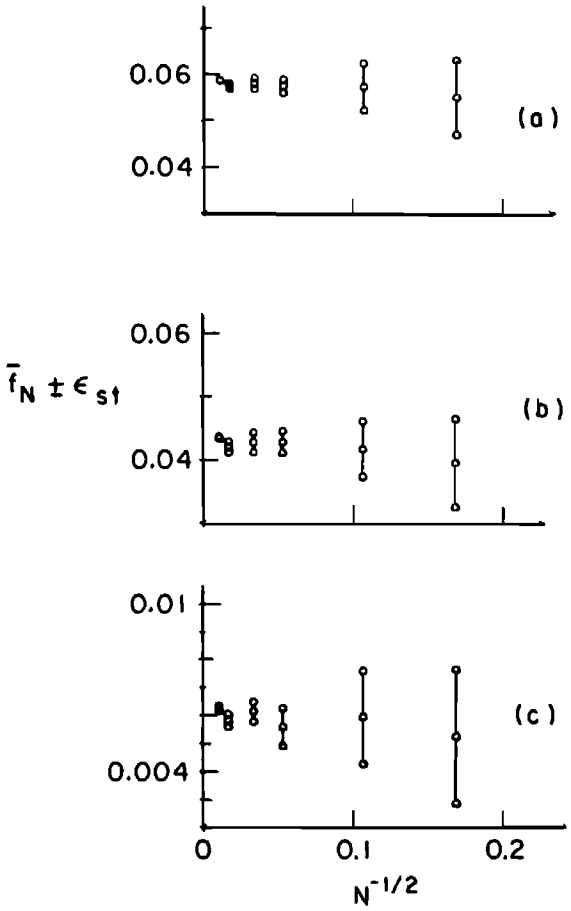

FIGURE 4 Expectation of ensemble-average of f against $N^{-1/2}$ at different radial locations: (a) $\eta=0.0$, (b) $\eta=0.692$, (c) $\eta=1.615$. Error bars show plus and minus the standard error.

Figure 4 also shows that, as expected, ε_{st} increases linearly with $N^{-1/2}$. Simple statistical arguments suggest that the standard error in $\langle f\rangle_N$ scales with $[\widetilde{f''^2}/N]^{1/2}$. In order to examine this suggestion, the normalized standard error

$$\varepsilon_{st}^* \equiv \varepsilon_{st} N^{1/2}/f_{N'}, \tag{27}$$

is plotted against η in Figure 5. It appears that ε_{st} does scale with $[\widetilde{f''^2}/N]^{1/2}$, and the normalized standard error ε_{st}^* is of order 3. For $N=4{,}000$ and $N=10{,}000$, ε_{st}^* is estimated from just two samples ($M=2$). The scatter seen on the figure is not surprising therefore.

These numerical results confirm the convergence of the Monte Carlo method (as $N\to\infty$) and allow the statistical error to be estimated. Inverting Eq. (27), dividing by $\tilde{f}_0$ (the centerline value of $\tilde{f}$), and replacing $f_{N'}$ by $[\widetilde{f''^2}]^{1/2}$, we obtain

$$\varepsilon_{st}/\tilde{f}_0 \approx N^{-1/2}\,\varepsilon_{st}^*[\widetilde{f''^2}]^{1/2}/\tilde{f}_0. \tag{28}$$

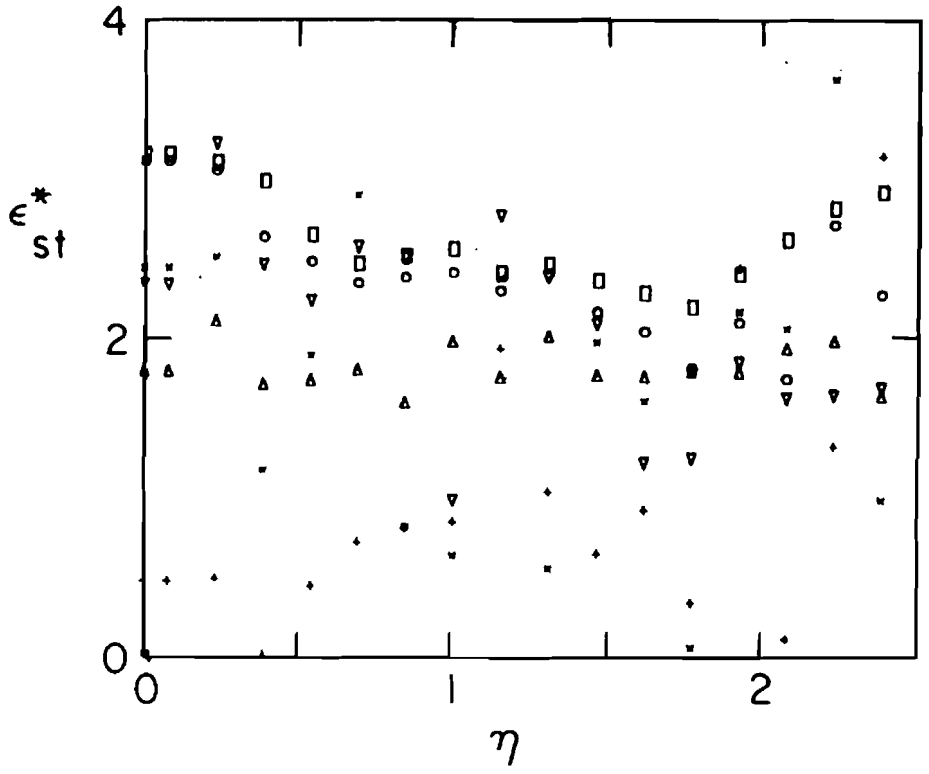

FIGURE 5 Normalized standard error against normalized radial distance: $N=40$, □; $N=100$, ○; $N=400$, △; $N=1{,}000$, ▽; $N=4{,}000$, ×; $N=10{,}000$, +.

And taking $\epsilon_{st}^* \approx 3$ and $[\widetilde{f''^2}]^{1/2}/\tilde{f}_0 \approx 0.3$ we obtain the estimate

$$\epsilon_{st}/\tilde{f}_0 \approx N^{-1/2}. \tag{29}$$

For the different values of N, Table II shows this estimate and also the calculated value of $\epsilon_{st}/\tilde{f}$ on the centerline. It may be seen that Eq. (29) provides a good (slightly conservative) estimate.

TABLE II

Statistical error estimates and computer run times

N	(ϵ_{st}/f_0) calculated	ϵ_{st}/f_0 Eq. (29)	CPU time per run (minutes)
40	0.142	0.158	4.2
100	0.088	0.1	4.6
400	0.025	0.05	8.5
1,000	0.021	0.032	17.3
4,000	0.011	0.016	63.4
10,000	0.0015	0.01	155.4

Also shown in the table are the CPU times required to perform the Monte Carlo calculations on an IBM 4341. Apart from a small overhead, the CPU time increases linearly with N.

(After these test calculations were performed, a mistake in implementing the small mean axial pressure gradient was detected in the code. This error has a small effect on the mean velocity but is of no consequence in the context of these numerical tests. The error was corrected prior to the performance of the calculations reported in the next section.)

4 RESULTS AND DISCUSSION

Calculations were made for three flows: an isothermal, inert methane jet discharging into quiescent air (Birch *et al.*, 1978); a hydrogen/air diffusion flame (Kent and Bilger, 1973); and a hydrogen–argon/air diffusion flame (Driscoll *et al.*, 1982). For each flow, the Monte Carlo calculation was performed three times (using different random numbers) and the results reported were obtained by averaging over the three runs. There were 1,000 elements at each of 28 grid nodes. The grid extended to $\eta_{max}=4.0$ and the axial step size was $\Delta X=0.1$. Based on the numerical results of the last section, the statistical error is estimated to be about 2 percent. Each run required about 15 min CPU time on an IBM 4341.

4.1 *Initial Conditions*

Initial conditions for the dependent variables $\tilde{U}$, k, ε and $\tilde{p}(\hat{f})$ are specified at $x=0$. In the jet, $f=1$ and hence $\tilde{p}(\hat{f})$ is a delta function at $\hat{f}=1$. Similarly, in the quiescent surroundings or co-flowing airstream, $\tilde{p}(\hat{f})$ is a delta function at $\hat{f}=0$. For the two diffusion flames, the initial profile of $\tilde{U}$ is taken from the experimental data of Kent and Bilger (1973), while for the inert methane jet, a one-seventh power law is assumed corresponding to fully-developed turbulent pipe flow.

There is always some uncertainty and ambiguity in specifying initial profiles of k and ε. Here, k and ε are determined from the ordinary differential equations

$$\frac{1}{r}\frac{d}{dr}\left(r\frac{\mu_T}{\sigma_k}\frac{dk}{dr}\right)+G'-\langle\rho\rangle\varepsilon-\langle\rho\rangle k/\tau=0, \tag{30}$$

and

$$\frac{1}{r}\frac{d}{dr}\left(r\frac{\mu_T}{\sigma_\varepsilon}\frac{d\varepsilon}{dr}\right)+C_{\varepsilon 1}\frac{\varepsilon}{k}G'-C_{\varepsilon 2}\langle\rho\rangle\frac{\varepsilon^2}{k}-\langle\rho\rangle\varepsilon/\tau=0, \tag{31}$$

where

$$G'\equiv\mu_T\left(\frac{d\tilde{U}}{dr}\right)^2. \tag{32}$$

The time scale τ is specified by a two-step procedure. First, these equations are solved with τ set to infinity. Then τ is specified to be the value of k/G' (obtained from the first solution) at the radial location at which G' is maximum. The equations are solved a second time with this value of τ and the resulting profiles of k and ε are

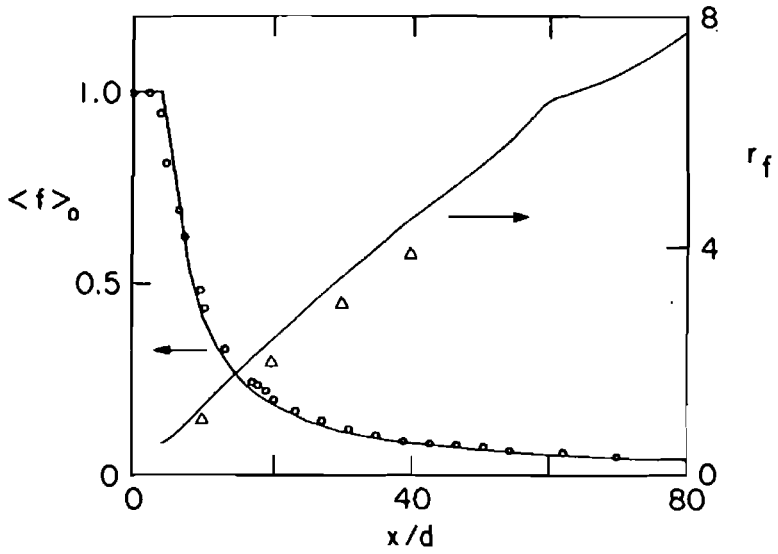

FIGURE 6 Mean centerline mixture fraction and mixture fraction half-width against normalized axial distance: ○, △ experiments, Birch *et al.* (1978), ——— calculations.

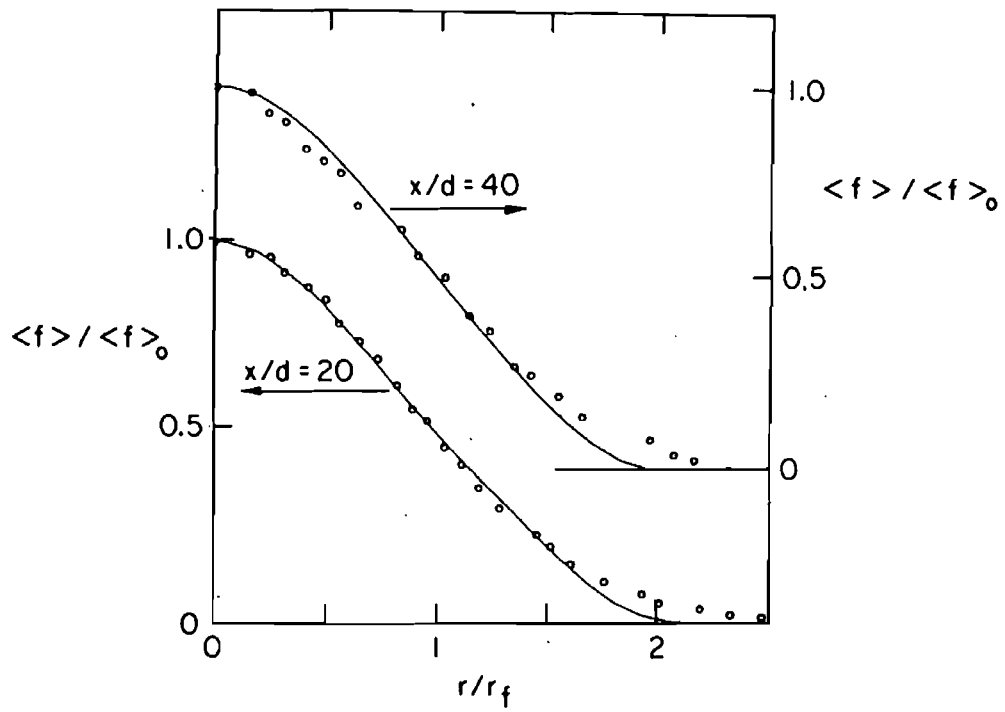

FIGURE 7 Normalized mean mixture fraction against normalized radial position at $x/d=20$ and $x/d=40$. (Symbols as Figure 6.)

taken as the initial conditions. This procedure yields plausible initial conditions and removes the ambiguity in their specification.

In order to investigate the sensitivity of the Monte Carlo solutions to the initial conditions, Nguyen (1984) performed two calculations for the methane jet—one with the initial conditions described above, and one with top-hat profiles of k and ε. At $x/d=10$ the differences in mean quantities between the two calculations are typically 10 percent: beyond $x/d=30$ the differences are negligible.

4.2 *Inert Methane Jet*

Birch *et al.* (1978) used a laser-Raman technique to measure the methane concentration in a turbulent jet of methane discharging into quiescent air. The experimental data are of conventionally-averaged quantities—$\langle f\rangle$, $\langle (f')^n\rangle$, $(n=2, 3, 4)$ and $p(f)$. Consequently the calculations are also reported as conventional averages.

Figure 6 shows the axial variation of $\langle f\rangle_0$—the mean mixture fraction $\langle f\rangle$ on the jet centerline—and it may be seen that there is excellent agreement between the calculations and the experimental data. (Here and henceforth the subscript 0 denotes a centerline value.) Also shown is the axial variation of the mixture fraction half-width r_f which is defined as the radial distance at which $\langle f\rangle$ is half of its centerline value. The calculated spreading rate dr_f/dx is about 15 percent greater than the measured value of 0.095. This discrepancy is most likely due to the known inaccuracy of the k–ε turbulence model in calculating the spreading rate of axisymmetric jets (Pope, 1978). The calculated normalized profiles of $\langle f\rangle$ are in good agreement with the data, Figure 7, except at the edge of the jet where the measured profiles extend beyond those calculated.

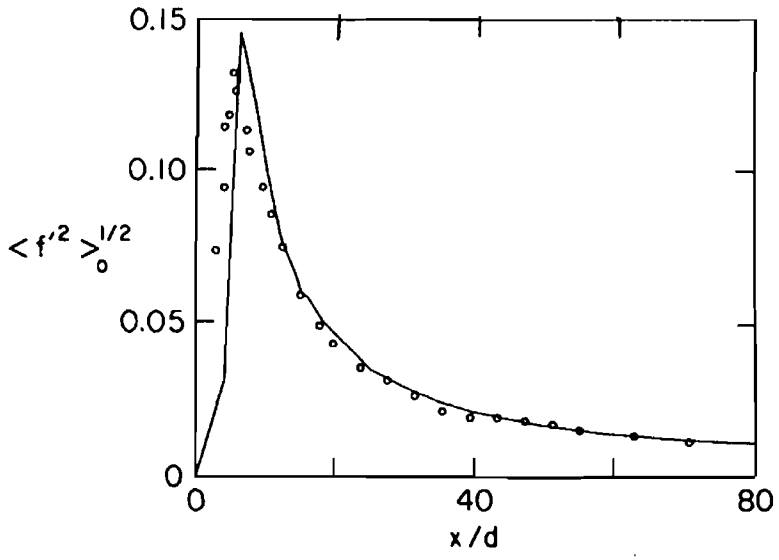

FIGURE 8 Standard deviation of centerline mixture fraction against normalized axial distance. (Symbols as Figure 6.)

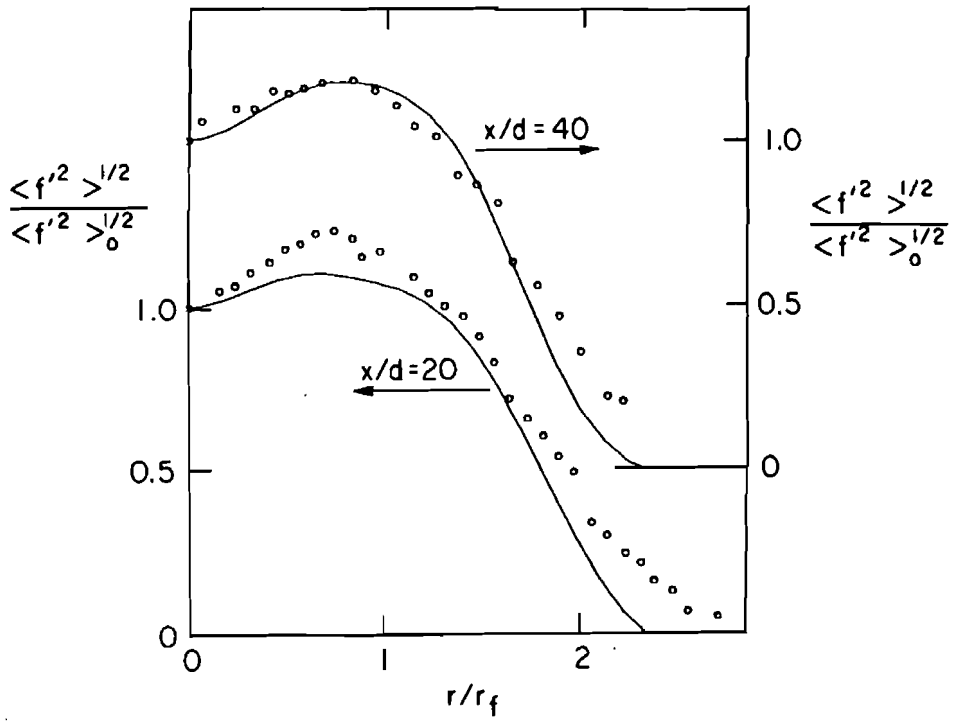

FIGURE 9 Standard deviation of mixture fraction against normalized radial distance at $x/d=20$ and $x/d=40$. (Symbols as Figure 6.)

Axial and radial profiles of the standard deviation of f are shown in Figures 8 and 9. In general there is good agreement with the data.

Radial profiles of the skewness $S \equiv \langle f'^3 \rangle / \langle f' \rangle^{3/2}$ and the flatness or kurtosis $K \equiv \langle f'^4 \rangle / \langle f'^2 \rangle^2$ are shown in Figures 10 and 11. In accord with the data, the calculations show a small negative skewness close to the centerline and large positive values at the edge. But at the edge, the magnitude of the calculated skewness is two to three times greater than that measured. On the centerline the measured kurtosis is close to the Gaussian value of 3 whereas the calculated value is about 4.0. The value of K rises towards the edge of the jet and, again, the calculated values are significantly greater than those measured.

The calculations of the skewness and flatness factor are a sensitive test of the mixing model. It is known that for the case of decaying fluctuations in homogeneous turbulence, Curl's mixing model predicts that K grows without bound, rather than tending to the Gaussian value of 3 (Pope, 1982). Thus the discrepancies at the edge of the jet are to be expected. It is likely that the use of an improved mixing model (Pope, 1982) would substantially reduce these discrepancies.

Calculated and measured pdf's of methane mole fraction $p(\xi)$ at $x/d=10$ are compared in Figure 12. Since there are small discrepancies between calculated and measured profiles of $\langle f \rangle$ and $\langle f'^2 \rangle$, the calculated pdf's are reported, not at the same radial location as the measurements, but at the location where the calculated

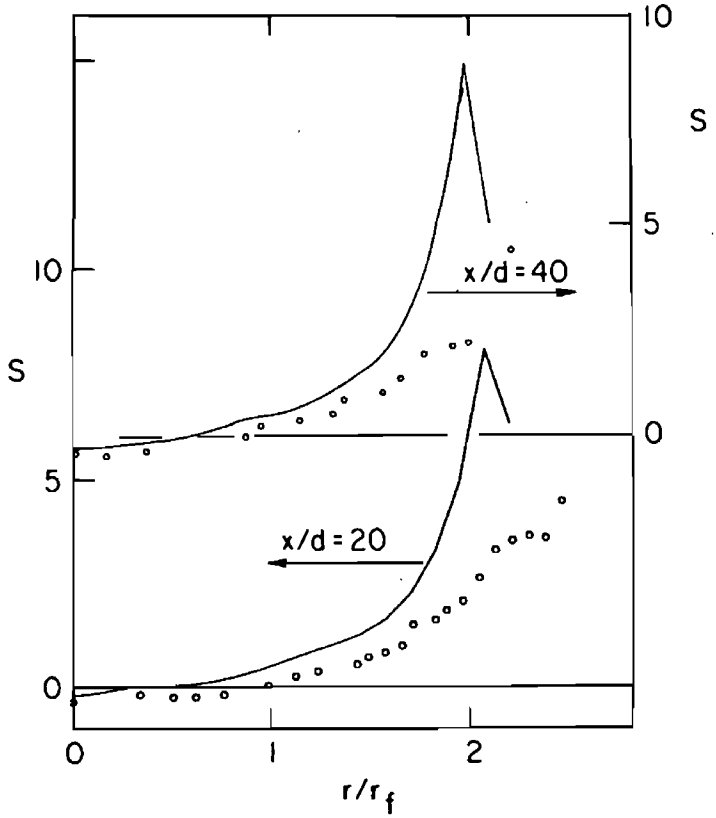

FIGURE 10 Skewness of f against normalized radial distance at $x/d=20$ and $x/d=40$. (Symbols as Figure 6.)

and measured values of $\langle f \rangle$ and $\langle f'^2 \rangle$ are about the same. This provides a better comparison of pdf shapes.

There is good agreement between the calculated and measured pdf's. On the centerline the pdf is a bell-shaped curve, but at $r/d \approx 1.7$ it is bimodal. At the outermost location there is a spike at $\xi = 0$ corresponding to ambient fluid.

4.3 *Hydrogen/Air Diffusion Flame*

Kent and Bilger (1973) made measurements in a flame formed by a hydrogen jet burning in a co-flowing stream of air. Measurements were made for the four velocity ratios (jet to co-flowing stream) of 2, 5, 8 and 10 to 1. Additional measurements on the same apparatus have been made by Glass and Bilger (1978), by Bilger and Beck (1975), and by Kennedy and Kent (1981). Calculations are reported for the velocity ratio 10:1 for which most data are available.

Figure 13 shows the mean centerline velocity normalized by the jet exit centerline velocity U_j. There is good agreement between calculated and measured profiles. [The calculated profile appears to have a discontinuous slope and a potential core is not evident. These are artifacts of the plotting: although the calculations were made with a small axial step size ($\Delta X = 0.1$), the axial profiles are plotted as straight lines between calculated points some distance apart.]

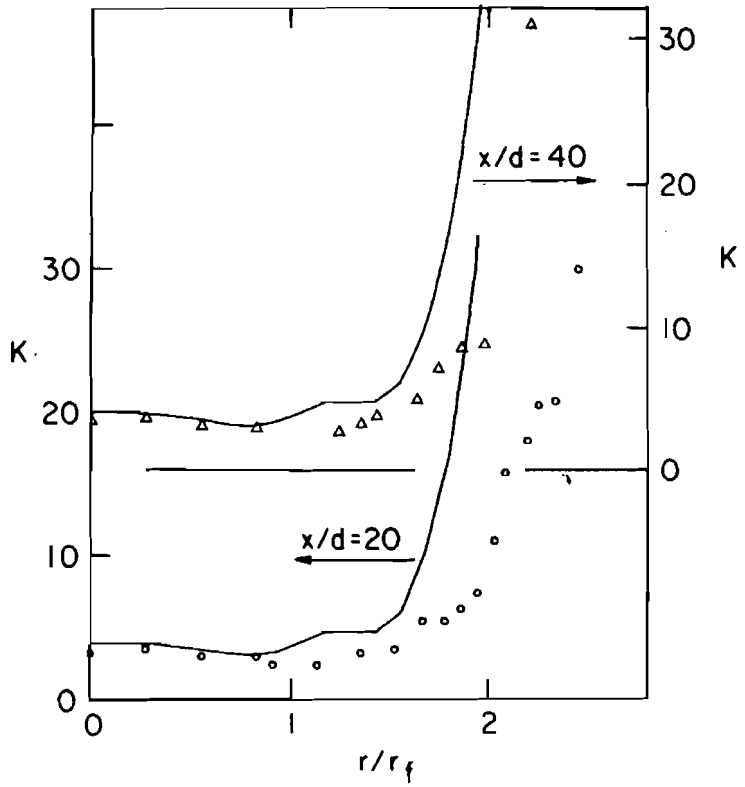

FIGURE 11 Kurtosis of f against normalized radial distance at $x/d=20$ and $x/d=40$. (Symbols as Figure 6.)

Figure 14 shows the axial variation of the centerline mean temperature and mole fractions. Radial profiles of these quantities at $x/d=40$ are shown in Figure 15. Axial and radial profiles of $\tilde{f}$ are shown in Figures 16 and 17. The half-width r_f at $x/d=40$ (used in the normalization in Figure 17) is calculated to within a few percent of the measured value. All these profiles show a close agreement between calculations and measurements.

Figure 18 shows the calculated normalized standard deviation of f on the centerline compared to three different sets of data. Kennedy and Kent (1981) using Mie scattering measured values at least twice of those calculated. On the other hand, the data of Kent (1972) and of Drake *et al.* (1982) (albeit for a different flame) are in fair agreement with the calculations. These observations add weight to Drake *et al.*'s suggestion that the Mie-scattering measurements are in error. In spite of this, the calculated normalized radial profile at $x/d=55$ (Figure 19) agrees well with Kennedy and Kent's data.

Calculated pdf's at $x/d=55$ are compared with Kennedy and Kent's data in Figure 20. In this case the calculations are reported at the grid node closest to the measurement location. It is apparent that the measurements show a greater probability of small values of f than do the calculations. The large measured values of $\tilde{p}(\hat{f})$ for small $\hat{f}$ most likely account for the larger standard deviation (see Figure 18).

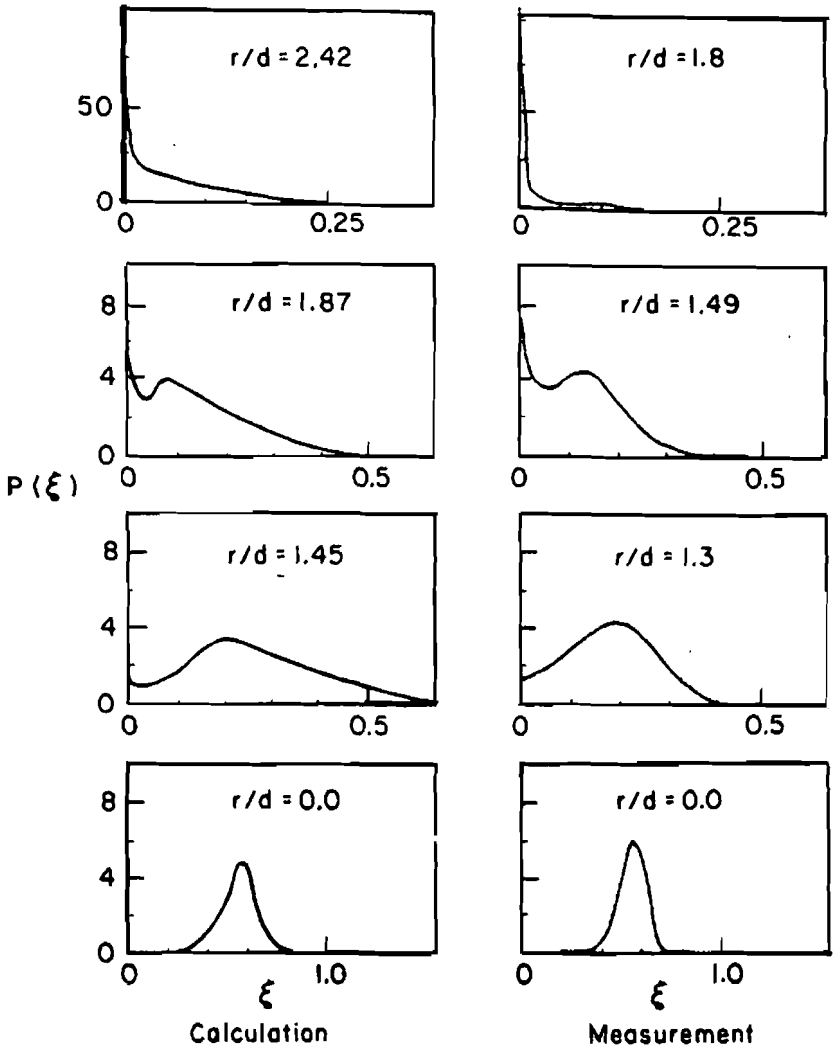

FIGURE 12 Pdf's of methane mole fraction at $x/d=10$: measurements of Birch *et al.* (1978).

Additional results are reported by Nguyen (1984). These include profiles of mean velocity, mean momentum flux $\langle \rho U^2 \rangle$, and turbulence intensity, as well as profiles of quantities reported here but at other axial locations. The level of agreement between these calculations and measurements is comparable to that exhibited in Figures 13–20.

4.4 *Hydrogen–Argon/Air Diffusion Flame*

Dibble *et al.* (1982) and Driscoll *et al.* (1982) report measurements of a jet diffusion flame that is geometrically similar to that of Kent and Bilger but in which the fuel

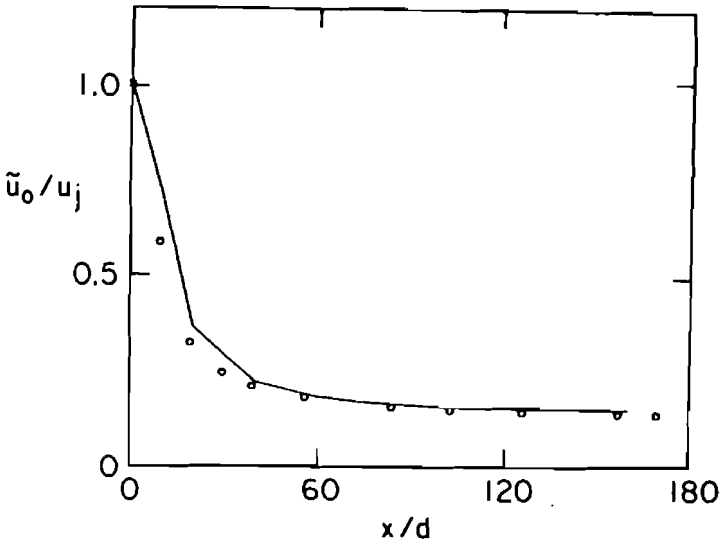

FIGURE 13 Normalized centerline mean velocity against normalized axial distance: ○ experiments, Kent and Bilger (1973); ——— calculations.

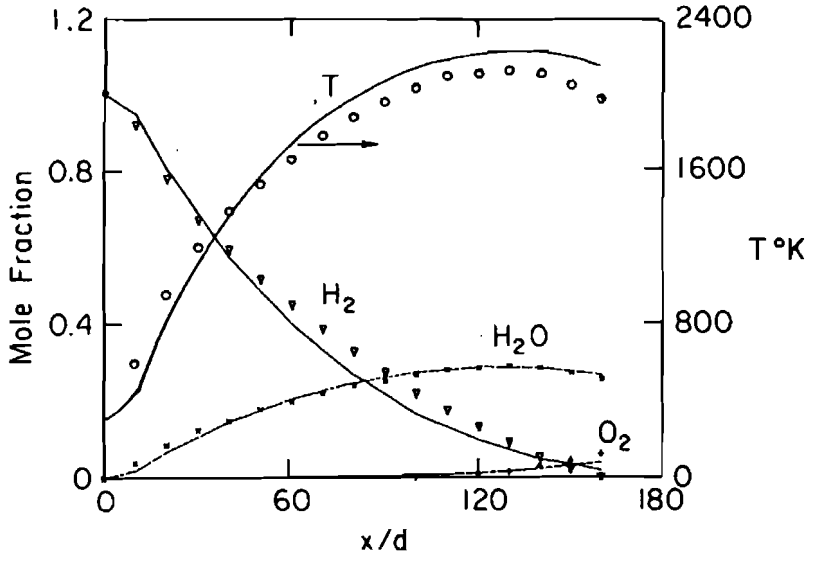

FIGURE 14 Centerline mean temperature and mole fractions against normalized axial distance: symbols, measurements of Kent and Bilger (1973); lines, calculations.

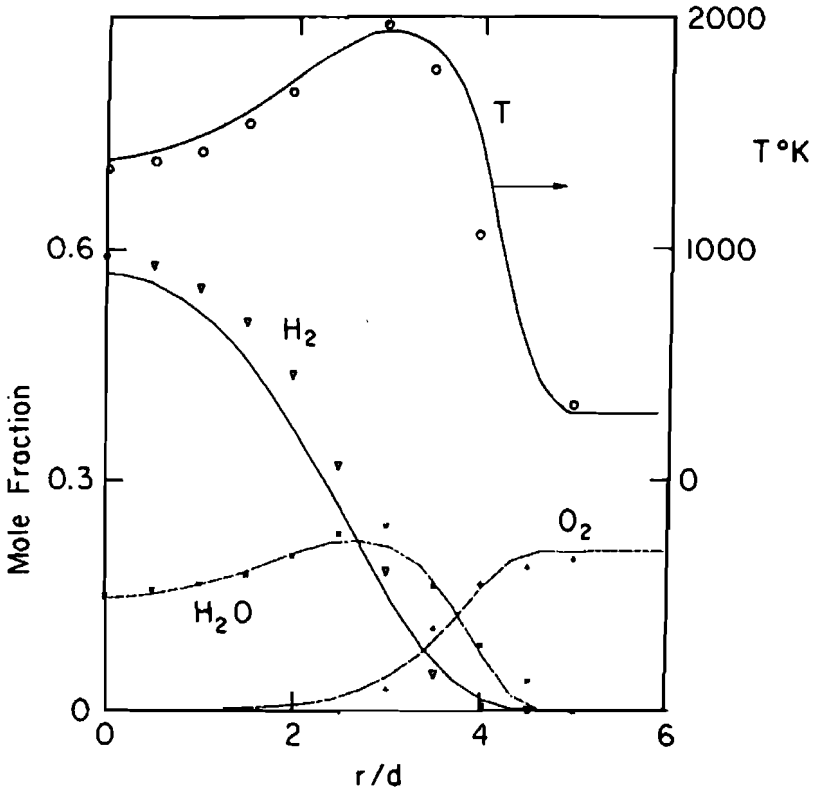

FIGURE 15 Mean temperature and mole fractions against normalized radial distance at $x/d=40$. (Symbols as Figure 14.)

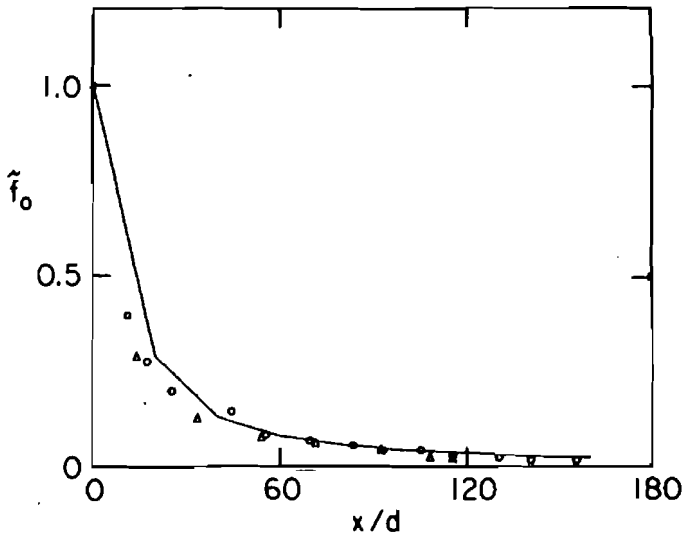

FIGURE 16 Mean centerline mixture fraction against normalized axial distance: measurements ○, Kent and Bilger (1973), △, Kennedy and Kent (1981); ———, calculations.

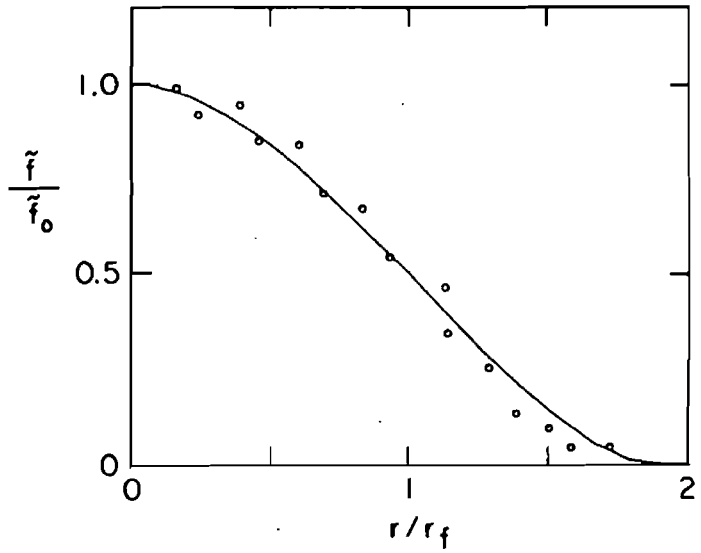

FIGURE 17 Normalized mean mixture fraction against normalized radial distance at $x/d=40$. (Symbols as Figure 13.)

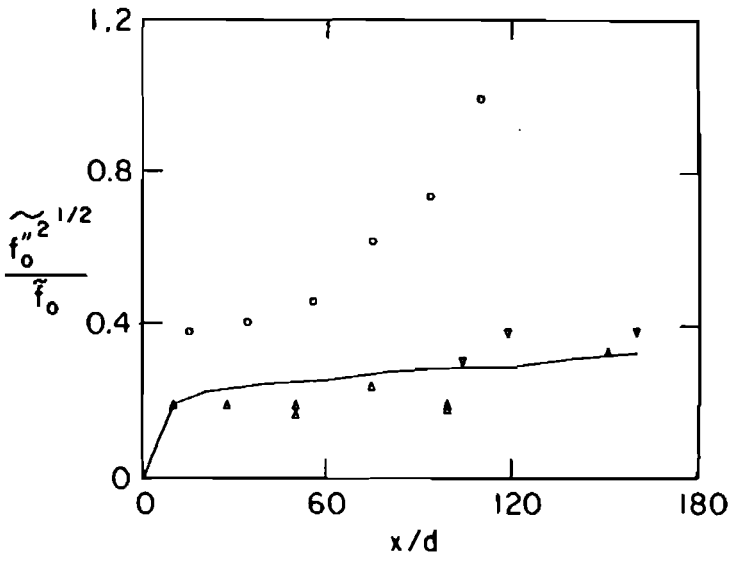

FIGURE 18 Normalized mixture fraction rms against normalized axial distance: measurements ○, Kennedy and Kent (1981), △, Drake *et al.* (1982), ▽, Kent (1972); ———, calculations.

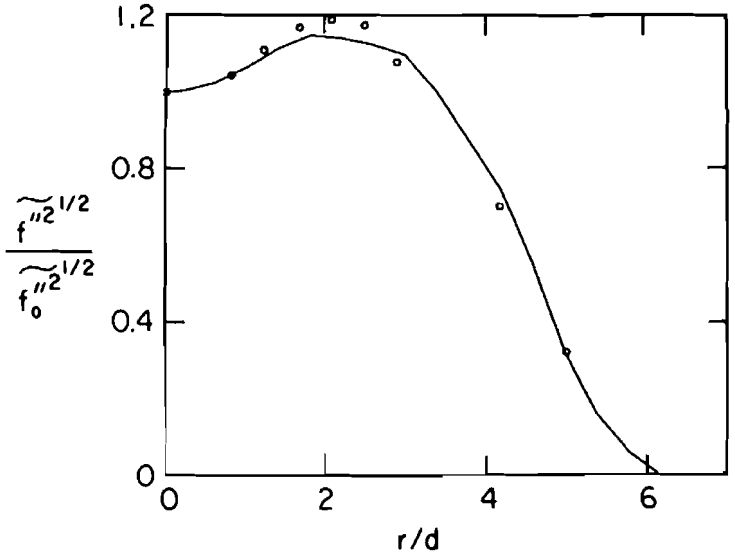

FIGURE 19 Normalized mixture fraction rms against normalized radial distance at $x/d=55$: measurements ○, Kennedy and Kent (1981); ——, calculations.

is a mixture of 78 percent hydrogen and 22 percent argon. The jet to co-flowing stream velocity ratio is 18.1:1. Compared to pure hydrogen, this fuel has a higher density and a higher stoichiometric mixture fraction (0.162 compared to 0.028).

There are questions concerning the reliability of some of the data of Driscoll *et al.* First, the centerline velocity in the jet nozzle U_j is reported to be equal to the bulk flow velocity $\bar{U}$: but for the geometry of the apparatus one would expect fully developed turbulent pipe flow with $U_j/\bar{U}\approx 1.2$. Second, at $x/d=5$, the centerline mean velocity and density are reported to be 20 and 30 percent less than their initial values. Even though the length of the potential cores in low density jets are known to be shorter than the constant-density value of 8 diameters, such rapid decreases in $\tilde{U}_0$ and $\langle\rho\rangle_0$ are nevertheless surprising and in need of confirmation.

In an attempt to compensate for these problems, Kollmann (1982) shifted the experimental data by 5 diameters when comparing them to his calculations (Kollmann, private communication): we follow this practice. Thus we compare our calculations at $x/d=15$, for example, with the data reported at $x/d=10$. (The x/d values given below and in the figures refer to the calculations).

Figure 21 shows the mean excess centerline velocity $\tilde{U}_0-U_\infty$, where U_∞ is the velocity of the co-flowing airstream. Except far downstream, the agreement between calculations and measurements is poor. For example, at $x/d=35$ the calculated excess velocity is almost twice that measured. The radial profiles at $x/d=55$ (Figure 22) also show poor agreement. At other axial locations (not shown) the agreement is similar, except at $x/d=15$ where it is yet worse (see Nguyen, 1984).

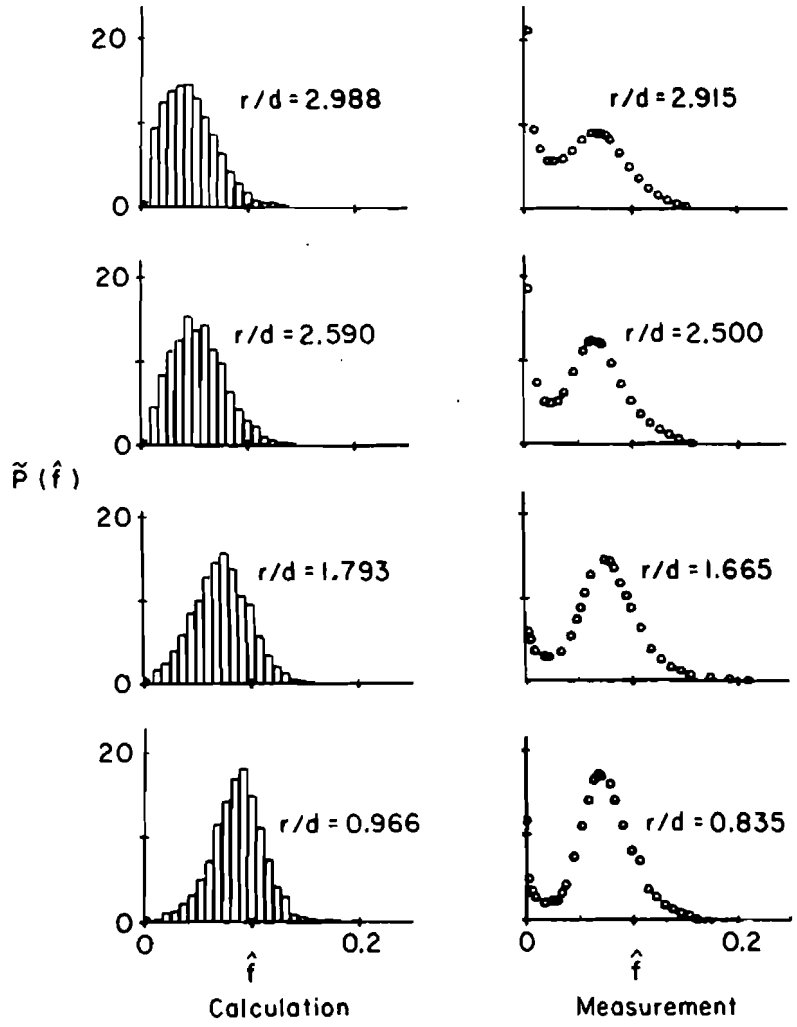

FIGURE 20 Mixture fraction pdf's at $x/d=55$: measurements of Kennedy and Kent (1981).

The centerline rms velocity fluctuations are plotted in Figure 21. (The calculated value is obtained by assuming that the normal stresses are equal.) It appears that the calculations fall slightly below the data, although there is some scatter, at $x/d=75$ in particular. (It should be noted that the calculated quantities in Figures 21 and 22 are density weighted, while the measurements are conventional averages: but it is estimated that the difference between the two averages is quite small.)

The axial variation of the mean centerline density is shown in Figure 23, and radial profiles are shown in Figures 24 and 25. The agreement between calculations

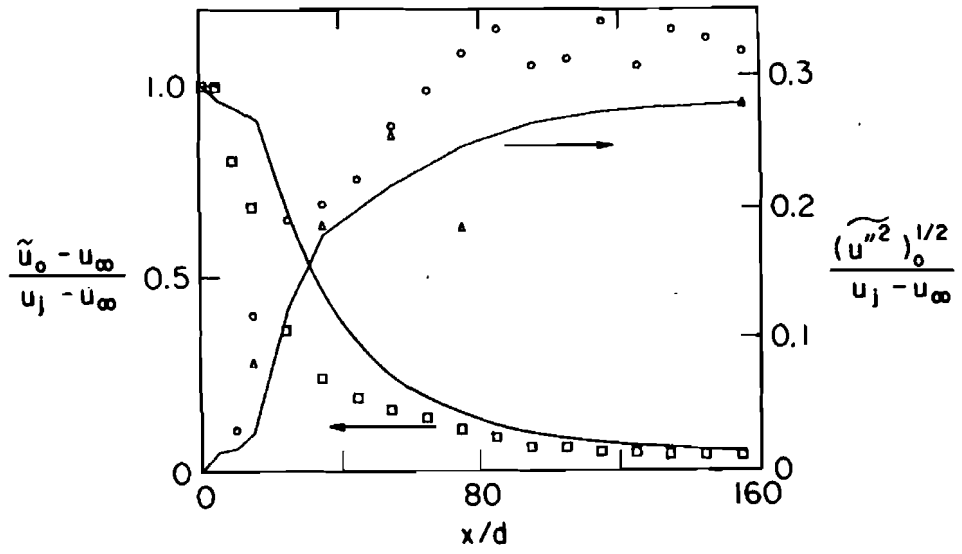

FIGURE 21 Normalized excess centerline mean and rms velocity against normalized axial distance: measurements, Driscoll *et al.* (1982), □, ○ from axial profiles, △ from radial profiles; ——, calculations.

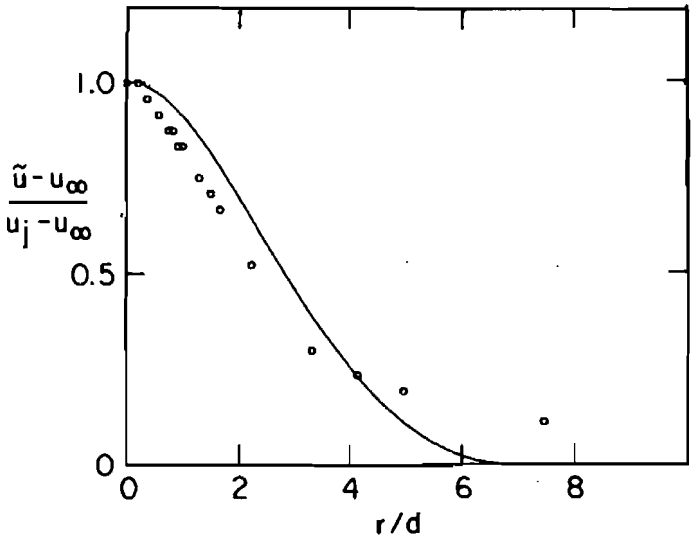

FIGURE 22 Normalized mean axial velocity at $x/d = 55$ against normalized radial position: ○, measurements, Driscoll *et al.* (1982); ——, calculations.

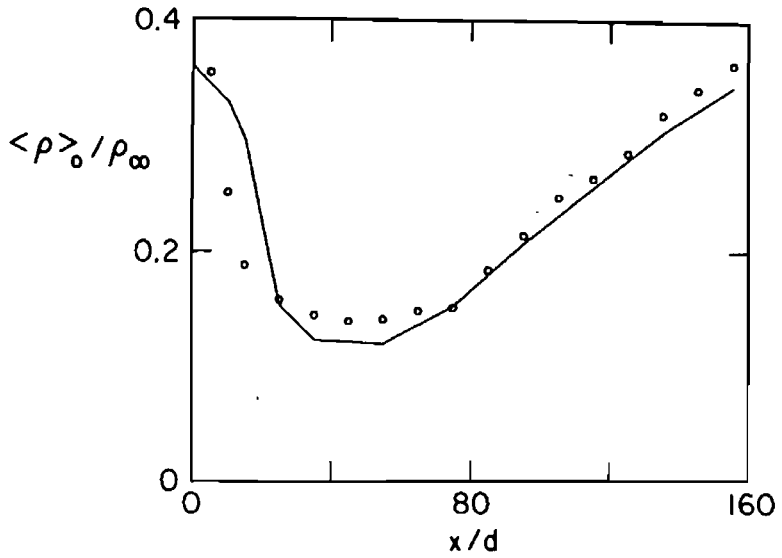

FIGURE 23 Normalized mean centerline density against normalized axial distance. (Symbols as Figure 22.)

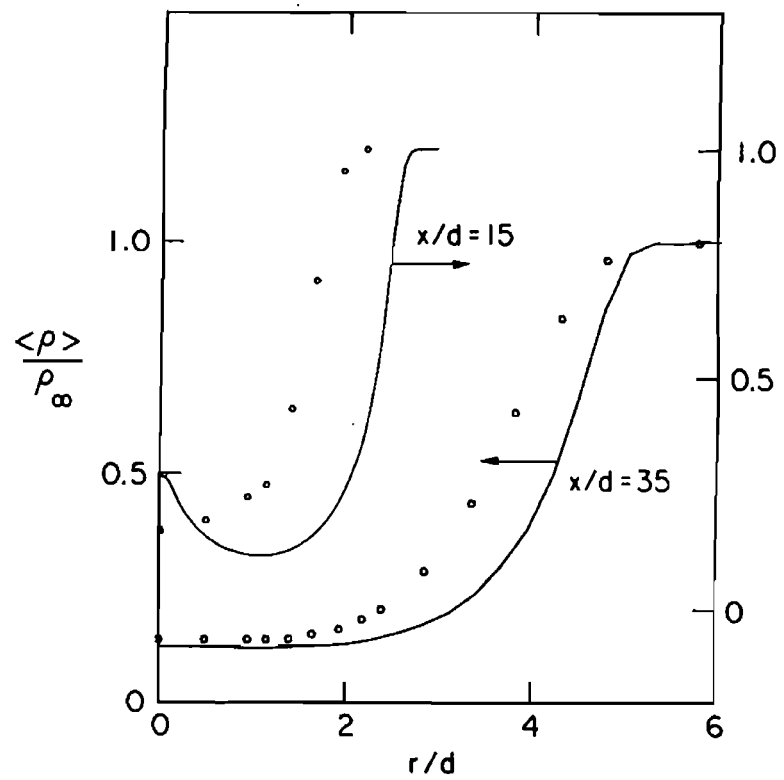

FIGURE 24 Normalized mean density against normalized radial distance at $x/d=15$ and 35. (Symbols as Figure 22.)

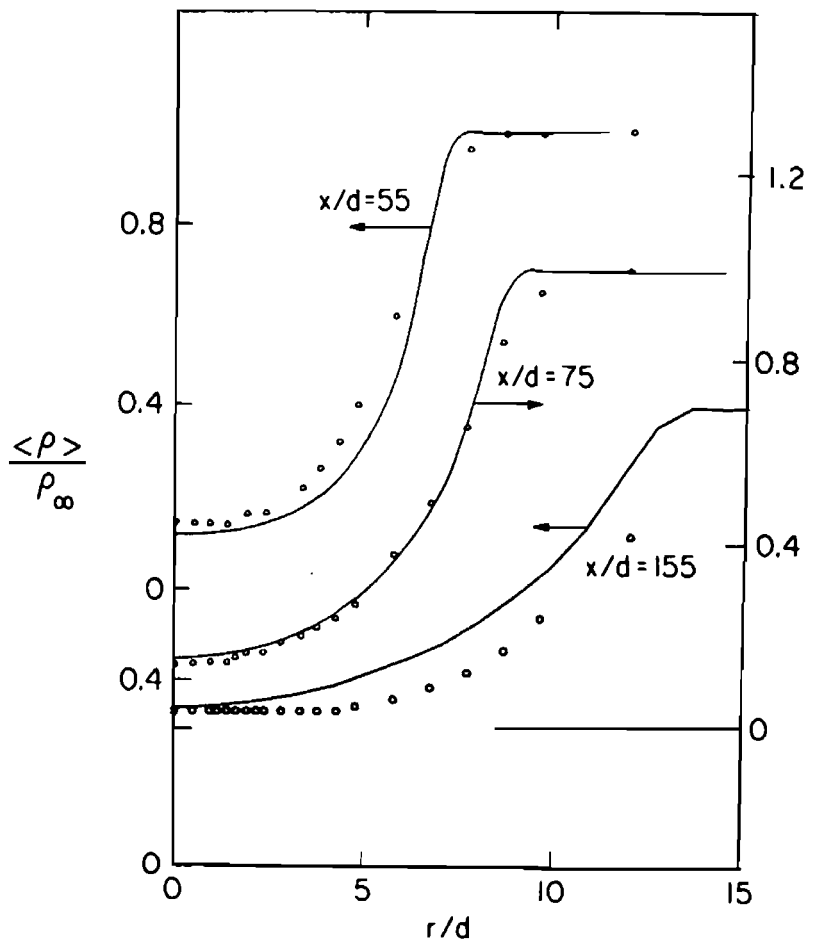

FIGURE 25 Normalized mean density against normalized radial distance at $x/d=55$, 75 and 155. (Symbols as Figure 22.)

and measurements is poor at $x/d=15$, but is quite good thereafter. The profiles at $x/d=55$ and 75 (and, to a lesser extent, those at $x/d=35$ and 155) show that the width of the flame is calculated quite accurately at these axial locations.

Radial profiles of the standard deviation of the density are shown in Figure 26. At the two farthest locations ($x/d=75$ and 155) the agreement between calculations and measurements is good. At $x/d=35$ and 55, two discrepancies are apparent: the maximum value of $\langle\rho'^2\rangle^{1/2}/\langle\rho\rangle$ is calculated to be about 50 percent greater than that measured (although the location of the peak is calculated correctly); and in the center of the flame ($r/d<2$), the calculated values of $\langle\rho'^2\rangle^{1/2}/\langle\rho\rangle$ fall significantly below the measured value of 0.2. The latter discrepancy could be due to experimental error from a variety of sources in this low density region—shot noise, background

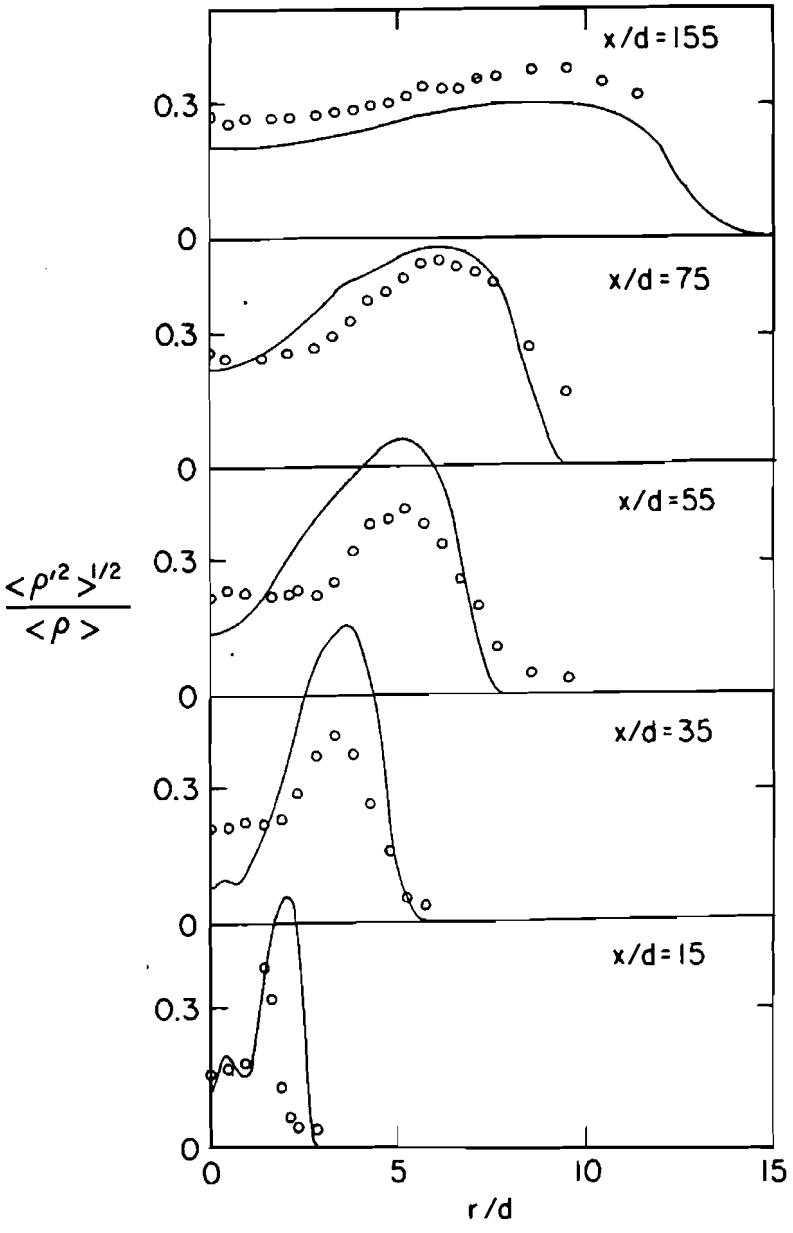

FIGURE 26 Normalized rms density against normalized radial distance. (Symbols as Figure 22.)

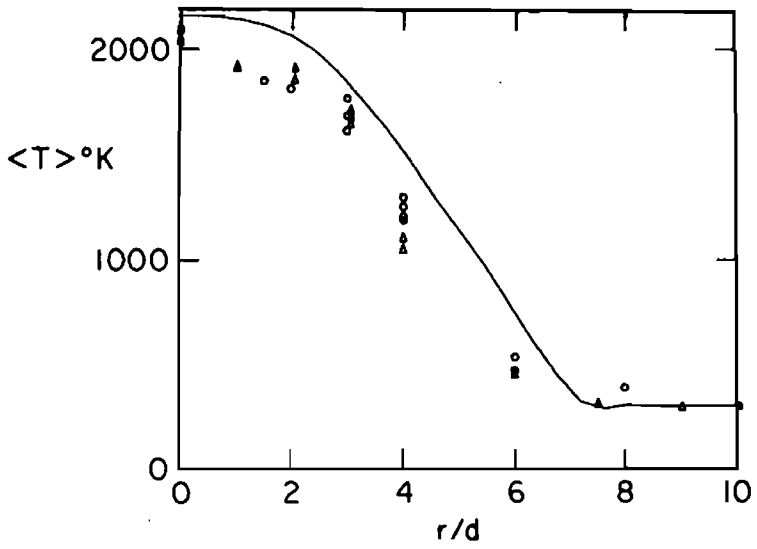

FIGURE 27 Mean temperature against normalized radial distance at $x/d=55$: ○, △, measurements, Dibble *et al.* (1982); ———, calculations.

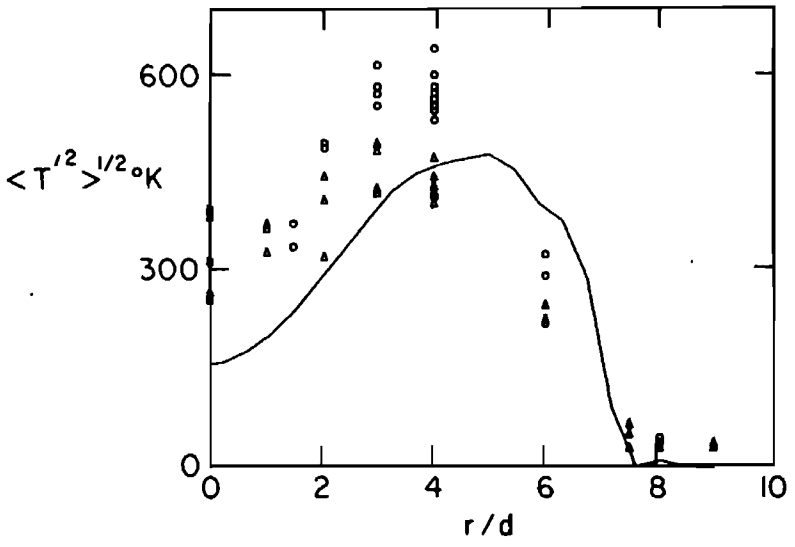

FIGURE 28 Mean temperature against normalized radial distance at $x/d=55$: ○, △, measurements, Dibble *et al.* (1982); ———, calculations.

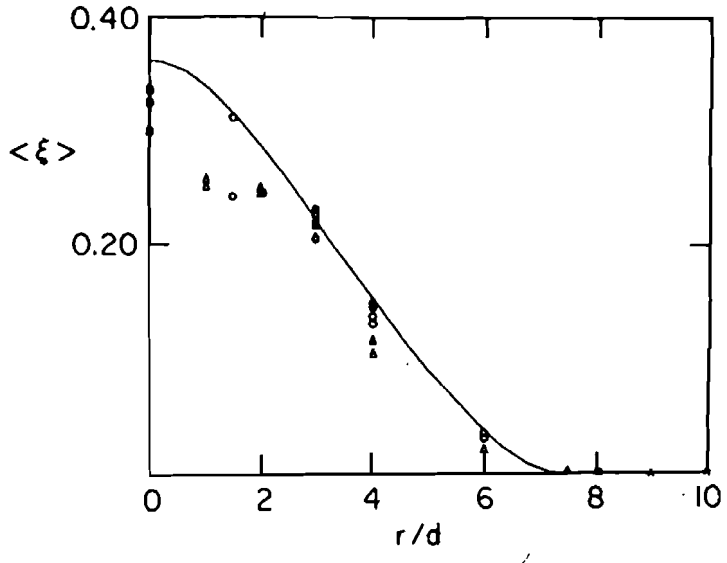

FIGURE 29 Mean atomic mixture mole fraction against radial distance at $x/d=55$. (Symbols as Figure 27.)

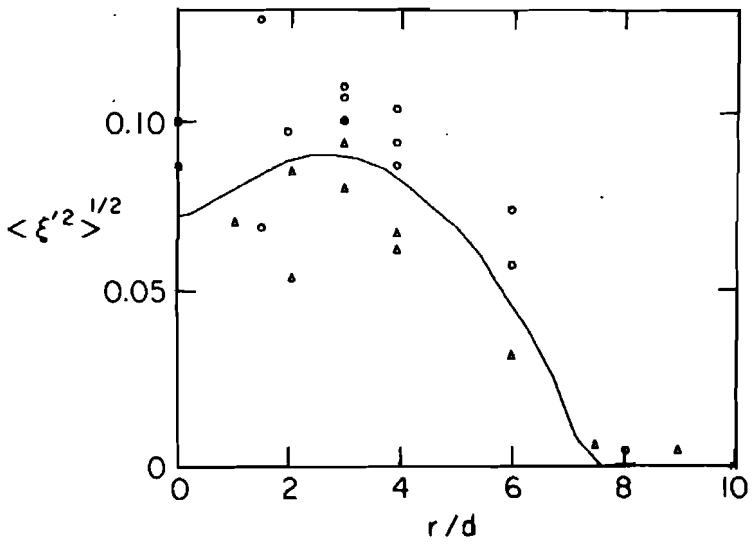

FIGURE 30 Rms atomic mixture mole fraction against radial distance at $x/d=55$. (Symbols as Figure 27.)

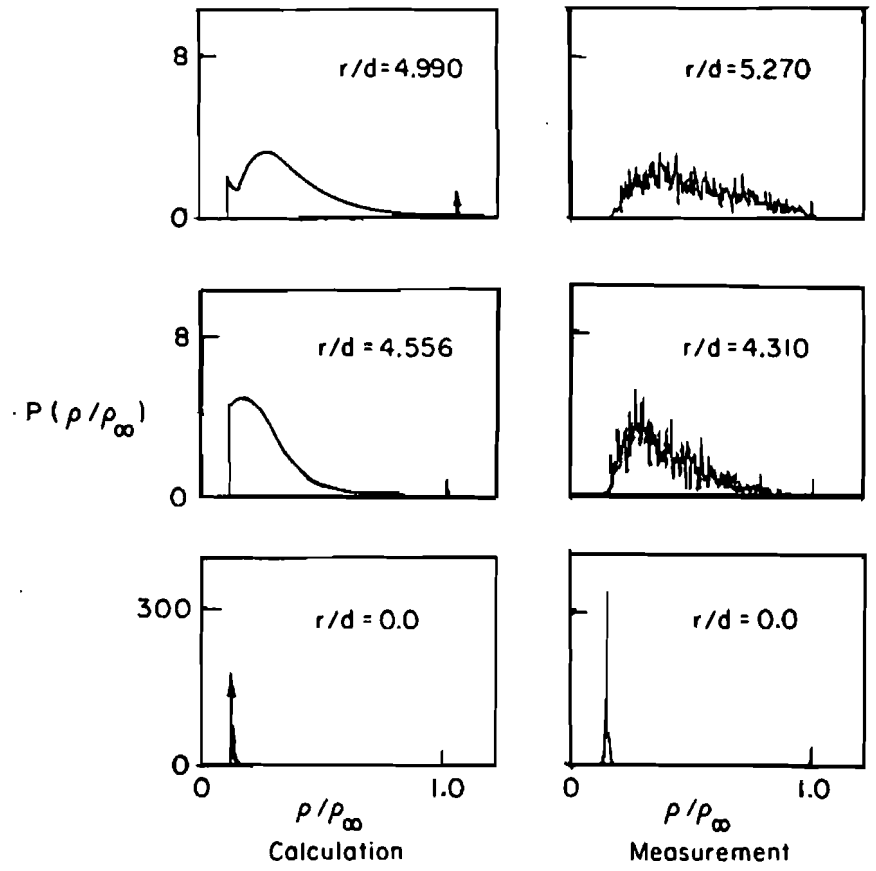

FIGURE 31 Probability density functions of normalized density at $x/d=55$: measurements of Driscoll *et al.* (1982). (*Continued on p. 43*).

scattering, for example (Dibble, private communication). As with other quantities, the agreement at $x/d=15$ is poor.

Figures 27–30 show the radial profiles at $x/d=55$ of the mean and rms temperature T and mixture mole fraction ξ. There is reasonable agreement between calculations and measurements.

Probability density functions of density are shown in Figure 31. These are at $x/d=55$ and, again, the calculated pdf's are reported at the grid node closest to the measurement station. The pdf's show a variety of shapes. From the centerline outward the pdf's are: a spike at $\rho/\rho_\infty \approx 0.13$; positively skewed pdf's; fairly flat pdf's; a negatively skewed pdf; and a spike at $\rho/\rho_\infty = 1$. The spike on the centerline arises because ρ varies little with f (or ξ) for the range of f (or ξ) values found at that location. The broadness of the measured pdf at $r/d=9.58$ is most likely due to measurement noise (see Bilger, Antonia and Sreenivasan, 1976). There is at least a qualitative agreement between the calculated and measured pdf's.

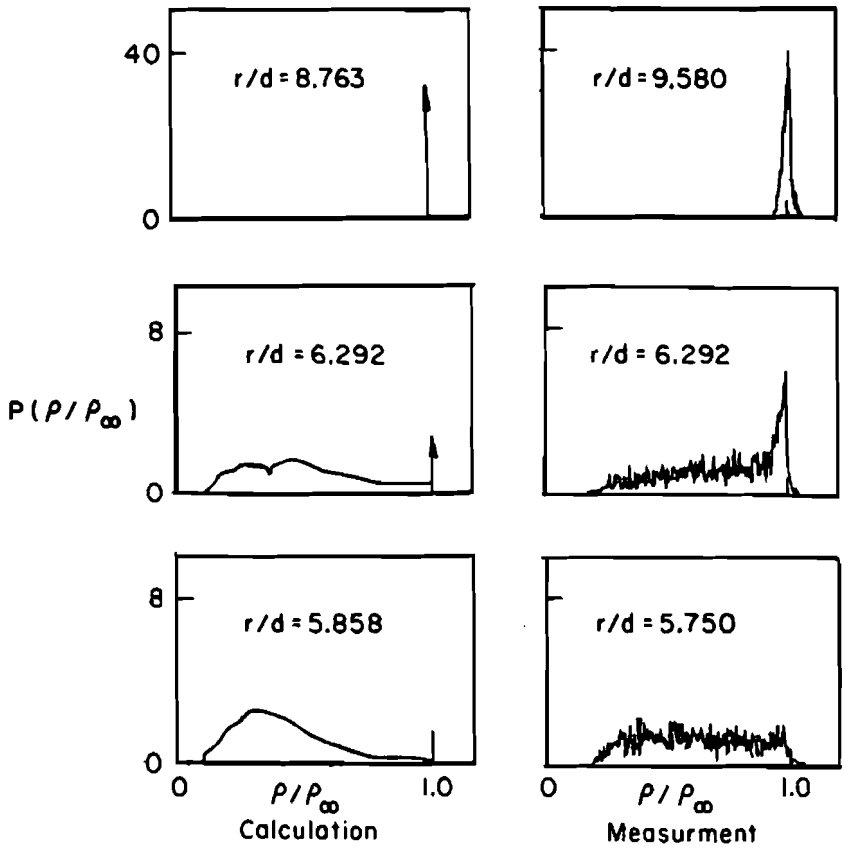

FIGURE 31 (*continued*)

CONCLUSION

A numerical model has been used to calculate the properties of turbulent diffusion flames. The mean continuity and momentum equations are solved by a finite-difference method, as are the modelled transport equations for k and ε. The conserved scalar approach is used with the assumption of rapid reaction so that the thermochemical state is uniquely related to the mixture fraction $f(x, t)$. A modelled transport equation for the mixture fraction pdf is solved by a Monte Carlo method.

Numerical tests have been performed on the Monte Carlo method to determine the statistical error as a function of N—the number of representative elements at each grid node. The test results confirm that the statistical error decreases as $N^{-1/2}$. For $N = 3{,}000$ the statistical error is about 2 percent and the CPU time required is 45 minutes on an IBM 4341.

The calculations for an inert methane jet, in general, show good agreement with the data of Birch *et al.* (1978). However, the mixture fraction skewness and kurtosis are significantly overpredicted at the edge of the jet, due to the inadequacy of Curl's

mixing model. Nevertheless there is good qualitative agreement between calculated and measured pdf shapes.

For the two turbulent diffusion flames considered, the level of agreement with data is quite good and comparable to that obtained in previous modelling studies (Kent and Bilger, 1976; Kollmann, 1982, for example). Again there is good qualitative agreement between calculated and measured pdf shapes.

The modelling could be improved in three respects: the use of an improved mixing model (Pope, 1982) would decrease the discrepancies in skewness and kurtosis; gradient-diffusion assumptions could be avoided by solving a modelled equation for the joint pdf of velocity and mixture fraction (Pope, 1981c); and, the edges of the jets could be treated more realistically by taking explicit account of intermittency (Pope, 1984).

For the pdf of a single variable, the modelled transport equation could be solved by a finite-difference method as easily as by a Monte Carlo method—indeed this has been done by Janicka *et al.* (1978). But for joint pdf's of several variables, Monte Carlo methods remain computationally practicable whereas finite-difference methods do not. Thus, the present method can readily be extended to treat finite-rate reactions and unequal diffusivities, in which case several scalar variables are required.

ACKNOWLEDGEMENT

This work was supported by the National Science Foundation (Engineering Energetics Program) grant numbers CPE 8000026 and CPE 8207790. The present address of T. V. Nguyen is Boeing Aerospace Co., P.O. Box 3999, Seattle, WA 98124.

REFERENCES

Bilger, R. W., Antonia, R. A., and Sreenivasan, K. R. (1976). Determination of intermittency from the probability density function of a passive scalar. *Physics of Fluids* **19**, 1471.

Bilger, R. W., and Beck, R. E. (1975). Further experiments in turbulent jet diffusion flames. *Fifteenth Symposium (International) on Combustion*, The Combustion Institute, p. 541.

Birch, A. D., Brown, D. R., Dodson, M. G., and Thomas, J. R. (1978). The turbulent concentration field of a methane jet. *Journal of Fluid Mechanics* **88**(3), 431.

DeBoor, C. (1978). *A Practical Guide to Splines*, Springer-Verlag, New York.

Curl, R. L. (1963). Dispersed phase mixing. I. Theory and effects in simple reactors. *AIChE Journal* **9**, 175.

Dibble, R. W., Kollmann, W., and Schefer, R. W. (1982). Conserved scalar fluxes measured in a turbulent non-premixed flame by combined laser Doppler velocimetry and laser Raman scattering. Presented at the 1982 Fall Meeting of the Western States Section of the Combustion Institute.

Dopazo, C. (1979). Relaxation of initial probability density functions in the turbulent convection of scalar fields. *Physics of Fluids* **22**, 20.

Drake, M. C., Bilger, R. W., and Starner, S. H. (1982). Raman measurements and conserved scalar modeling in turbulent diffusion flames. *Nineteenth Symposium (International) on Combustion*, The Combustion Institute, p. 545.

Driscoll, J. F., Schefer, R. W., and Dibble, R. W. (1982). Mass fluxes $\overline{\rho' u'}$ and $\overline{\rho' v'}$ measured in a turbulent non-premixed flame. *Nineteenth Symposium (International) on Combustion*, The Combustion Institute.

Givi, P. Sirignano, W. A., and Pope, S. B. (1984). Probability calculations for turbulent jet flows with mixing and reaction of NO and O_3. To be published in *Combustion Science and Technology*.

Glass, W., and Bilger, R. W. (1978). The turbulent jet diffusion flame in a co-flowing stream—some velocity measurements. *Combustion Science and Technology* **18**, 165.

Gordon, S., and McBride, B. J. (1971). Computer program for calculations of complex chemical equilibrium compositions, rocket performance, incident and reflected shocks, and Chapman–Jouguet detonations. NASA SP-273.

Hawthorne, W. R., Weddell, D. S., and Hottel, H. C. (1949). Mixing and combustion in turbulent gas jet. *Third Symposium (International) on Combustion, Flame and Explosion Phenomena*, The Combustion Institute, p. 266.

Janicka, J., Kolbe, W., and Kollmann, W. (1979). Closure of the transport equation for the probability density function of turbulent scalar fields. *Journal of Non-Equilibrium Thermodynamics* **4**, 47.

Janicka, J., Kolbe, W., and Kollmann, W. (1978). The solution of a pdf-transport equation for turbulent diffusion flames. *Proc. 1978 Heat Trans. Fluid Mech. Inst., Stanford University.*

Jones, W. P., and Whitelaw, J. H. (1982). Calculation methods for reacting turbulent flows: a review. *Combustion and Flame* **48**, 1.

Kennedy, I. M., and Kent, J. H. (1981). Scalar measurements in a co-flowing turbulent diffusion flame. *Combustion Science and Technology* **25**, 109.

Kent, J. H. (1972). Turbulent jet diffusion flames. Ph.D. Thesis, University of Sydney.

Kent, J. H., and Bilger, R. W. (1976). The prediction of turbulent diffusion flame fields and nitric oxide formation. *Sixteenth Symposium (International) on Combustion*, The Combustion Institute, p. 1643.

Kent, J. H., and Bilger, R. W. (1973). Turbulent diffusion flames. *Fourteenth Symposium (International) on Combustion*, The Combustion Institute, p. 615.

Kolbe, W., and Kollmann, W. (1980). Prediction of turbulent diffusion flames with a four equation turbulence model. *Acta Astronautica* **71**, 91.

Kollmann, W. (1982). Prediction of density–velocity correlations in turbulent diffusion flames. Presented at the 1982 Fall Meeting of the Western States Section of the Combustion Institute.

Launder, B. E., and Spalding, D. B. (1976). *Mathematical Models of Turbulence*, Academic Press, London.

Lockwood, F. C., and Naguib, A. S. (1975). The prediction of the fluctuations in the properties of free, round jet, turbulent, diffusion flames. *Combustion and Flame* **24**, 109.

Nguyen, T. V. (1984). Monte Carlo calculations of turbulent diffusion flames. Ph.D. Thesis. Massachusetts Institute of Technology.

Pope, S. B. (1984). Calculations of a plane jet. *AIAA Journal* **22**, 896.

Pope, S. B. (1982). An improved turbulent mixing model. *Combustion Science and Technology* **28**, 131.

Pope, S. B. (1981a). A Monte Carlo method for the pdf equations of turbulent reacting flows. *Combustion Science and Technology* **25**, 159.

Pope, S. B. (1981b). Monte Carlo calculations of premixed turbulent flames. *Eighteenth Symposium (International) on Combustion*, The Combustion Institute, p. 1001.

Pope, S. B. (1981c). Transport equation for the joint pdf of velocity and scalars in turbulent flow. *Physics of Fluids* **24**, 588.

Pope, S. B. (1978). An explanation of the turbulent round-jet/plane-jet anomaly. *AIAA Journal* **16**, 279.

Pope, S. B. (1977a). A novel calculation procedure for free shear flows, Imperial College Report FS/77/7.

Pope, S. B. (1977b). A calculation procedure for two-dimensional free shear flows: the SPEAR computer program. Imperial Report FS/77/17.

Reinsch, C. H. (1967). Smoothing by spline functions. *Numerische Mathematik* **10**, 177.

Rhodes, R. P., Harsha, P. T., and Peters, C. E. (1974). Turbulent kinetic energy analyses of hydrogen–air diffusion flame. *Acta Astronautica* **1**, 443.